www.sciencemag.org/content/343/6169/422/suppl/DC1

Supplementary Materials for

Visualization of Dynamics of Single Endogenous mRNA Labeled in Live Mouse

Hye Yoon Park, Hyungsik Lim, Young J. Yoon, Antonia Follenzi, Chiso Nwokafor, Melissa Lopez-Jones, Xiuhua Meng, Robert H. Singer*

*Corresponding author. E-mail: robert.singer@einstein.yu.edu

Published 24 January 2014, *Science* **343**, 422 (2014)
DOI: 10.1126/science.1239200

This PDF file includes:

Materials and Methods
Supplementary Text
Figs. S1 to S10
Captions for movies S1 to S8
References

Other supplementary material for this manuscript includes the following:

Movies S1 to S8

Acknowledgments

We thank the members of the Singer laboratory for discussions; K. Chen and Einstein Transgenic Mouse facility for lentiviral transgenesis; C. Montagna and Molecular Cytogenetic Core for DNA FISH; R. Sellers and Histology and Comparative Pathology facility for histopathology analysis; L. Ting and K. Kim for the help with IVIS Spectrum system; H. Cohen for the advice on statistical analysis; Molecular Biology facility at Janelia Farm Research Campus for identification of the transgene integration site. Microscopy equipment for the live cell imaging experiments was provided by the Analytical Imaging facility and Gruss Lipper Biophotonics Center. The Cancer Center Shared Resources were supported by National Cancer Institute (NCI) grant P30CA013330. H.Y.P. performed all of the experiments; H.L. and Y.J.Y. contributed to tissue imaging experiments; A.F. contributed to lentiviral transgenesis; C.N. and M.L.J. provided animal care and breeding; X.M. provided cloning of the constructs; H.Y.P., H.L., and R.H.S. wrote the manuscript; and R.H.S. provided overall supervision of the project.

Materials and Methods

Construction of lentiviral vectors and viral preparation

We generated a lentiviral vector (LV) that expresses NLS-HA-MCP-GFP under the control of the Ubiquitous C promoter (LV-MCP-GFP) by using the pCCLsin.PPT.UbiC.GFP.Wpre vector (*18*). Vesicular stomatitis virus G-glycoprotein (VSVG) pseudotyped lentiviral vector was produced by cotransfecting 293T cells with the third-generation packaging constructs, pMDLg/pRRE, pRSV-REV, pMD2.VSVG, and the transfer vector LV-MCP-GFP by calcium phosphate precipitation. The culture media was replaced with Iscove's modified Dulbecco's medium with 10% fetal bovine serum (FBS), 1% glutamax, and 0.25% penicillin-streptomycin (PS) at 12-16 hours after transfection. After 24 and 48 hours later, the supernatant was collected, filtered, and concentrated by unltracentrifugation at 20,000 rpm for 2 hours at 18°C. The LV pellet was resuspended in PBS and stored at -80°C in aliquots. The titer of LV was measured by transducing 293T cells with serial dilution of the vector stock and counting infected cells by flow cytometry.

Lentiviral transgenesis

All procedures using animals were performed in accordance with protocols approved by the Albert Einstein College of Medicine Institutional Animal Care and Use Committee (IACUC). LV-MCP-GFP with a titer of ~10^8 TU/mL was microinjected into the perivitelline space of single-cell embryos of C57BL/6J genetic background, which were subsequently implanted in the oviduct of pseudopregnant mice. The mice were genotyped by PCR using MCP forward primer, 5'- CCTGTAGCGTTCGTCAGAG-3' and GFP reverse primer, 5'-TGCTCAGGTAGTGGTTGTCG-3', yielding a ~840-bp product. PCR conditions were 95°C 45 s, 60°C 45 s, 72°C 45 s for 26 cycles. To screen the mice that express MCP-GFP protein, Western blots were performed on tail lysates using anti-GFP (1:2,500, GFP-1020; Aves Labs, Inc.) as a primary antibody, and anti-chicken IgG conjugated to IRDye 800 (1:10,000, Li-Cor Biosciences) as a secondary antibody. The MCP mouse line 4 was genotyped by PCR using a forward primer, 5'-CAATCTGTAGGTTGCTGTTTTGTCCTG-3' and two reverse primers, 5'-

ACATAGGCAGGAAAATCTTGAGTT-3', and 5'-TGGTTTCCCTTTCGCTTTCAG-3', yielding ~730-bp product for the WT allele and ~530 bp product for the transgenic allele. PCR conditions were 95°C 1 min, 55°C 1 min, 72°C 1 min for 34 cycles.

DNA fluorescence in situ hybridization

DNA in situ hybridization was carried out using the similar method described previously (*4*). About 300 µL of blood was collected from the retro-orbital sinus of the mice in heparinized tubes. Macrophages were cultured for ~3 days, and then cells in interphase were deposited on slides. The DNA probe was prepared by labeling the plasmid DNA harboring the MCP-GFP transgene with Spectrum Orange (Abbott Molecular, Des Plaines, IL). The slides were hybridized with the probe following a standard protocol (*19*), and counterstained with DAPI. The slides were imaged on an Olympus BX61 microscope equipped with an Olympus UPlanApo 100× 1.35 NA oil-immersion objective. Z-stacks with 0.2 µm step were collected and the maximum intensity projection image of the z-stack was produced using ImageJ. Nuclei were segmented using DAPI signal and the number of FISH spots within each nucleus was counted using particle detection software (*20*). The number of the integrated transgene was determined by calculating the average number of spots per nucleus.

Isolated organ fluorescence detection

C57BL/6J and MCP mice were fed with AIN-76A Rodent Diet (Research Diets Inc.) to reduce autofluorescence background. The isolated organs from adult mice were imaged with an IVIS Spectrum system (Caliper LifeSciences) in epifluorescence mode equipped with 465/30 nm and 520/20 nm filters for excitation and emission, respectively. The exposure time was optimized based on the level of fluorescence emitted from each organ.

Histology

All major organs and tissues were evaluated histologically by a board certified veterinary pathologist. The tissues included the liver, kidney, adrenal gland, spleen, heart, lungs with trachea and thyroid glands, esophagus, thymus, brain, small and large intestine, stomach, bladder, prostate, testes, bladder, bone marrow, spinal cord, skeletal muscles, skin, eyes, ears (outer, middle, and inner), oral and nasal cavity, and mesenteric lymph nodes. Samples were evaluated and graded based on a qualitative scale: 0, 1, 2, 3, 4, and 5, which correlated with no lesions, minimal, mild, moderate, marked, and severe lesions, respectively.

Western blotting

Whole-tissue extracts were separated on 4-12% Bis-Tris polyacrylamide precast gels in MOPS-SDS running buffer and transferred to membranes by using the iBlot dry blotting system following the manufacturer's instructions (Invitrogen). The following antibodies were used: Anti-HA (1:1,000, 11867423001; Roche Applied Science), anti-GFP (1:2,500, GFP-1020; Aves Labs, Inc.), anti-α-tubulin (1:2,500, 600-401-880, Rockland Immunochemicals, Inc.), anti-β-actin (1:5,000, A1978; Sigma), and anti-GAPDH (1:10,000, G9545; Sigma) as primary

antibodies, and anti-rat, anti-chicken, anti-rabbit, and anti-mouse IgG conjugated to IRDye 680 or 800 (1:10,000, Li-Cor Biosciences) as secondary antibodies. Western blots were scanned on the Odyssey infrared imaging system (Li-Cor Biosciences).

qRT-PCR

Total RNA was extracted using Trizol/chloroform (Invitrogen). cDNA was generated by reverse transcription using SuperScript III First-Strand Synthesis System (Invitrogen) with random hexamers. The amount of cDNA was quantified by real-time PCR using the following primer sets (mouse β-actin: FW 5'-CCACTGCCGCATCCTCTTCC-3', REV 5'-CTCGTTGCCAATAGTGATGACCTG-3'; mouse GAPDH: FW 5'-CATGGCCTTCCGTGTTCCTA-3', REV 5'-GCGGCACGTCAGATCCA-3'). Real-time PCR was performed using 150 nM of each primer, 1:300 dilution of the cDNA reaction, and SYBR Green PCR master mix (Applied Biosystems).

Single molecule RNA fluorescence in situ hybridization

Cells were grown on a coverslip and fixed in 4% paraformaldehyde in PBS for 20 min at room temperature. The coverslips were stored in 70% ethanol at 4°C for a few days and processed for fluorescence in situ hybridization (FISH) as described previously (*16*). Cells were hybridized with probes labeled with cy3 or cy5 dyes on the modified thymidine nucleotides marked with bold capital T.

MS2_LK51 probe:

TTTCTAGGCAA**T**TAGGTACCT**T**AGGATCTAA**T**GAACCCGGGAATAC**T**GCAG

MBA UTR-1 probe:
AGAAAGGG**T**GTAAAACGCAGC**T**CAGTAACAGTCCGCC**T**AGAAGCACT**T**GC

MBA UTR-2 probe:
GC**T**CCAACCAAC**T**GCTGTCGCCT**T**CACCGTTCCAG**T**TTTTAAATCC**T**G AG

MBA UTR-3 probe:
GGTGGC**T**TTTGGGAGGG**T**GAGGGACTTCCTG**T**AACCACTTATT**T**CATGGA

MBA UTR-4 probe:
CCCAGGGAGACCAAAGCC**T**TCATACATCAAGT**T**GGGGGGACAAAAAAAAG

MBA UTR-5 probe:
CAAAACAA**T**GTACAAAGTCC**T**CAGCCACATTTG**T**AGAACTTTGGGGGA**T**G

MBA e1_4102-50 probe:
G**T**GGACCGGCAACGAAGGAGC **T**GCAAAGAAGC**T**GTGCTCGCGGG**T**GGACG

Images were taken using an Olympus BX-61 microscope equipped with an X-cite 120 PC lamp (EXFO), a UPlanApo 100× 1.35 NA oil immersion objective (Olympus), and a CoolSNAP HQ CCD camera (Photometrics). Z-stack images of 0.2 μm step were taken with 100 ms exposure

time using MetaMorph software (Molecular Devices). Single mRNA detection was performed by using uTrack software (*20*). The sub-pixel positions and intensities of particles were quantified by a two-dimensional Gaussian fit. In z-stacks of single molecule FISH images, the same particles were tracked in the adjacent z-planes and the highest intensity was chosen for each particle as its intensity in the focused plane.

Primary fibroblast cultures

Primary fibroblasts were cultured from 13.5 days post coitum (dpc) embryos or from limb muscle of 0-2 day old pups from timed matings. The head, heart, and liver were removed from the embryos and the rest of the tissue was digested with Trypsin EDTA for 20 min. Cells were plated in culture medium (Dulbecco's modification of Eagle's medium (DMEM) supplemented with 10% FBS, 1% Glutamax, and 1% PS) for one hour and the unattached cells were washed off with fresh media. The next day, cells were plated on glass-bottom dishes (MatTek), and used for live-cell imaging within 48 hours.

Hippocampal neuron cultures

Dissociated hippocampal neuron cultures were prepared from 0-2 day old mouse pups using a method similar to that described previously (*21*). Briefly, we dissected out hippocampi, dissociated them with trypsin, and plated 85,000 cells onto poly-D-lysine-coated MatTek dishes (MatTek). The cultures were maintained in Neurobasal-A medium supplemented with B-27, Glutamax, and Primocin (Invivogen) at 37°C and 5% CO_2 for 1-22 days before use.

Epifluorescence live cell imaging

For live cell imaging, we removed the growth medium from cell cultures and replaced it with imaging media (phenol-red free L-15 medium containing 10% FBS, 1% Glutamax, 1% PS, and 1% oxyrase (Oxyrase, Inc.) for MEFs, and HEPES-buffered solution (HBS) containing 20 mM HEPES·HCl pH 7.4, 119 mM NaCl, 5 mM KCl, 2 mM $CaCl_2$, 2 mM $MgCl_2$, and 30 mM glucose for neurons) prior to the experiment. Wide-field images were taken on an Olympus IX-71 inverted microscope with a UApo 150× 1.45 NA oil immersion objective (Olympus), an MS-2000 XYZ automated stage (ASI), and an iXon electron-multiplying charge-coupled device (EMCCD) camera (Andor). The cells were kept at 37°C with 60% humidity in an environmental chamber (Precision Plastics). The GFP was excited by 488 nm line from an argon ion laser (Melles Griot). The emission was filtered with a 525/30 band-pass filter (Semrock). For single particle tracking, time-lapse images were taken in a single plane at 33 or 100 fps for MEFs and at 10 or 33 fps for neurons using stream acquisition mode in MetaMorph software (Molecular Devices). In order to count the number of mRNAs in the dendrites, z-sections were acquired with 0.3 μm step size using z-sweep acquisition mode in MetaMorph.

Preparation of brain slice and live tissue imaging

Mice at postnatal day 14-24 were deeply anesthetized with isoflurane. After decapitation, the whole brain was quickly removed and immersed into ice-cold, oxygenated (95% O_2 / 5% CO_2)

artificial cerebrospinal fluid (ACSF; 119 mM NaCl, 2.5 mM KCl, 1.3 mM $MgSO_4$, 2.5 mM $CaCl_2$, 1.0 mM NaH_2PO_4, 26.4 mM $NaHCO_3$, 11 mM D-glucose). Coronal sections (350-500 μm thick) were rapidly cut using a vibratome (Leica) and then transferred to a recovery chamber filled with oxygenated ACSF at room temperature. After recovery at room temperature for 1 hour, the slice was transferred to an imaging chamber (Warner Instruments Inc.) maintained at 32°C and continuously perfused (1 mL/min) with oxygenated ACSF.

Slices were imaged with a two-photon laser-scanning microscope (TPLSM) using a XLPlan N 25× 1.05 NA water immersion lens (Olympus). The excitation beam was short pulses from a mode-locked Ti:Sapphire laser at 880-nm wavelength with 100-fs duration and 80-MHz repetition rate. A Pockels cell was employed to attenuate the laser beam and also to rapidly switch it off during galvanometer's return travel. The average power was ~10 mW at the sample and the pixel dwell time was 4.4 μs. Fluorescence was detected with a 670DC dichroic beam splitter, an ET525/70 band-pass filter (Chroma Technology), and a GaAsP photomultiplier tube (PMT) detector (Hamamatsu) in the non-descanned mode. Images were acquired by using ScanImage software (*22*). Three images were averaged per frame and z-sections were acquired with 1 μm step size.

Image analysis

Particle detection and tracking were performed by using uTrack software (*20*). A two-dimensional Gaussian fit was performed to yield sub-pixel position and intensity of the particles. For single particle tracking, trajectories that were tracked for at least 10 consecutive frames were subject to the analysis. A custom-written MATLAB script was used to automatically classify each track into four different motion types: stationary, corralled, diffusive, and directed motions as described previously (*9, 23*). At an acquisition frequency of 33 fps, we determined particle localization precision to be ~50 nm by repetitive imaging of GFP-labeled mRNA molecules in a fixed cell. Because of this localization uncertainty, the mean squared displacement (MSD) of a fixed mRNP during five consecutive frames was ~0.025 μm^2. If the MSD of an mRNP in a live cell was less than 0.025 μm^2, we classified the particle as stationary (fig. S5, A and E). If a particle traveled in one direction for more than 1.5 μm, it was categorized as directed (fig. S5, D and H). The diffusion coefficient D of each individual track was determined by a linear fitting of the MSDs at $2\Delta t$, $3\Delta t$, and $4\Delta t$ weighted by error bars (*24, 25*). If the slope of the next three time-lag points in the MSD was less than D, the mRNP was classified as a corralled particle (fig. S5, B and F). The rest of the particles were considered as diffusive (fig. S5, C and G). The intensity of each particle was determined by the mean intensity of the track.

In order to quantify the directed transport of mRNP in neurons, we straightened dendritic segments using ImageJ Straighten plugin and generated kymographs using custom-written MATLAB scripts. The travel distance and velocity were calculated from the kymographs. Merge and split of mRNA were analyzed by manual counting in the kymographs followed by inspection of the time-lapse images. If the distance between two particles became shorter than ~250 nm for at least 10 s, it was counted as a merge event. If a diffraction-limited spot divided into two resolved spots for at least 10 s, it was counted as a split event. The intensities of mRNA particles in cultured neurons were quantified from the maximum projection of z-sweep images.

In live-tissue images, particles were detected in each plane of the z-stack with 1 μm step size. In the dendritic regions, the intensity histogram of the detected particles exhibited a sharp peak of

single mRNAs and a broad peak of mRNPs containing multiple copies of mRNAs (Fig. S10B). By using a two-component Gaussian fitting, we calculated the mean intensity of single mRNAs. In order to count the number of nascent mRNAs, we divided the intensity of the transcription site by the intensity of single mRNA. Transcription sites were determined by manually examining the time-lapse images of the same nuclei and identifying two bright spots that are relatively immobile.

Supplementary Text

Generation of MCP mouse

MCP mice were generated using lentiviral transgenesis technique (*3*). We had previously made several attempts to generate a transgenic mouse expressing MCP-GFP by using conventional methods such as pronuclear injection and embryonic stem (ES) cell electroporation techniques. Although several founders were positive for transgene integration, none of them expressed the protein except for one founder that died without offspring. Since it was reasoned that the MCP-GFP transgene might be easily silenced in mice, we used a lentiviral vector (fig. S1A) to integrate the transgene in multiple loci with high efficiency (fig. S1B).

Expression of MCP-GFP was verified in various tissues by Western blot and whole organ imaging (fig. S1, C and D). Histologic analysis confirmed that there was no discernible abnormality in the MCP mouse compared to the C57BL/6J wild-type (WT) mouse.

We obtained 45 founder mice, 33 of which (73%) carried the transgene, but only 11 mice (24%) expressed the MCP-GFP fusion protein. Three lines, derived from founders 1, 4, and 9, were further expanded and used for the experiments. Among the F1 progenies from crosses of the founders and C57BL/6J wild-type (WT) mice, the transgene-positive genotype was found in 92% of line1 (n = 26), 100% in line 4 (n = 15), and 100% in line 9 (n = 18), respectively. We also screened the transgene-positive F1 mice by Western blot of tail lysate, detecting MCP-GFP expression in 89% of line 1 (n = 24), 80% of line 4 (n = 15), and 100% of line 9 (n = 18). These results suggest that the transgenes were integrated in multiple chromosomes in these transgenic lines, but some of the transgenes were silenced. In order to breed the mice without reduction in the protein expression of MCP-GFP, we mated positive mice identified by Western blot of tail lysates. In MCP mouse line 4, an active MCP-GFP transgene was identified at ~2 kbp upstream of the Ube3a transcriptional start site on chromosome 7.

Quantification of β-actin mRNA localization in fibroblasts

By using single molecule FISH followed by the polarization-dispersion analysis (*26*), we confirmed that β-actin mRNA exhibits polarized localization in both WT and MCP×MBS primary fibroblasts (fig. S3, A-D). In this analysis, polarization index (PI) represents the deviation between the center of mRNA distribution and the center of the cell, and dispersion index (DI) measures the variance of mRNA distribution. The correlation coefficient R between PI and DI was -0.61 for WT (fig. S3C) and -0.40 for MCP×MBS primary fibroblasts (fig. S3D). The negative correlation coefficients between PI and DI indicate polarized localization of β-actin mRNA. The difference in the correlation coefficients of WT and MCP×MBS culture was within the variability of primary cultures from the same mouse strain, which was R = -0.47 ± 0.17 (SD) for the Actb-MBS mice (n = 4 culture preparations).

In contrast, a MEF cell line immortalized by SV40 T antigen did not exhibit polarized localization of β-actin mRNA (fig. S3, F and G). Moreover, even primary cells exhibited gradual loss of mRNA localization in a few days after isolation from mice (fig. S3E). Therefore we harvested primary MEFs from MCP×MBS mice and imaged them immediately within 48 hours to observe mRNA localization in live cells (Fig. 1B, fig. S6, and Movie S1-5). This has not been feasible in previous live-cell experiments using reporters since transfection was required.

Quantification of mRNA copy number

In order to count the copy number of β-actin mRNA molecules in each mRNP, we quantified the fluorescence intensity of mRNP particles by single molecule FISH (*16*). Immortalized MEFs from WT and Actb-MBS mice were fixed and hybridized with MS2_LK51 probe complementary to the 11 linkers between the MBS stem-loops (fig. S4, A and C). Using uTrack software (*20*), we detected significant local intensity maxima with an alpha-value of 0.1 and fit them with a two-dimensional Gaussian function in each section of a wide-field z-stack image. Then particles were tracked in the adjacent z-planes to find the intensity of each particle in the focused plane. The intensity histograms were generated for the particles detected in WT and Actb-MBS MEFs (fig. S4, B and D). Because there is no MBS sequence in WT MEF, particles detected in WT cells are non-specifically bound single probes. The intensity histogram of the single probes followed a normal distribution (fig. S4B). In Actb-MBS MEF, where each β-actin mRNA contains 11 binding sites for the probe, the intensity histogram showed two populations (fig. S4D). The low intensity population corresponds to single probes, and the high intensity population represents β-actin mRNP binding multiple MS2_LK51 probes. Using two-component Gaussian fitting, we estimated that the mean number of probes bound to each β-actin mRNP was 7 with a standard deviation of 4. Less than 1% of mRNP contained more than 11 probes (n = 1700 ± 300 mRNPs per cell).

The intensity distribution of β-actin mRNP consists of three major components: the distributions of 1) the intensity of a single probe, 2) the number of probes bound to a single β-actin mRNA, and 3) the copy number of β-actin mRNAs in each mRNP particle. First, 1) the intensity distribution of a single probe was measured as shown in fig. S4B, which was well approximated by a Gaussian distribution with the mean, μ = 1, and the variance, σ^2 = 0.4. If every particle binds a fixed number of probes, *k*, and if there is no covariance between the intensity of the probes, the particle intensity distribution will follow a Gaussian distribution with $\mu_k = k$ and $\sigma_k^2 = k\sigma^2$ (fig. S4E).

Next, we measured the hybridization efficiency of a probe to a single binding site in order to estimate 2) the distribution of the number of probes per mRNA. We performed two-color single molecule FISH on primary Actb-MBS fibroblasts using MBA e1_4102-50 probe labeled with Cy3 dyes and MS2_LK51 probe labeled with Cy5 dyes. MBA e1_4102-50 probe is complementary to only one binding site in the exon 1 of β-actin mRNA. We used Cy5-labeled MS2_LK51 probe to identify *a priori* locations of β-actin mRNAs. We found that 61% of the spots binding more than three MS2_LK51 probes were colocalized with MBA e1_4102-50 probes within the optical resolution (< 300 nm). Oligonucleotide probes that are about 50 bases long and have approximately 50% GC content work well in most cases using 50% formamide in the FISH protocol (*16*). Based on the similar nucleotide length and GC content percentage, we assumed that MS2_LK51 probe has the same 61% hybridization efficiency to its target sequence. If the binding events are independent of each other, we can calculate the binomial distribution of the number of MS2_LK51 probes binding to a single β-actin mRNA:

$$\Pr(X = k) = \frac{N!}{k!(N-k)!} p^k (1-p)^{N-k}$$

$$N = 11$$

$$p = 0.61$$

where k is the number of probes binding to a single mRNA molecule, N is the number of the probe binding sites per mRNA, and p is the hybridization efficiency (fig. S4F).

The intensity distribution of single β-actin mRNA is calculated from these two distributions (fig. S4, E and F) as shown in fig. S4G, which can be well approximated by a Gaussian distribution with the mean of 7 and the standard deviation of 3. This simulation result is in a good agreement with the experimental data in fig. S4D, suggesting that the mRNP particles in fibroblasts contain a single copy of β-actin mRNA. In addition, previous studies have provided substantial evidence for detecting single mRNA since the first demonstration of single molecule FISH (*16, 9, 27*).

We also quantified the intensity of GFP-labeled mRNA particles in primary MEFs cultured from MCP×MBS mice (Fig. 1B). The intensity histogram of particles shows only one population with a normal distribution (Fig. 1D). It was previously shown that the mean number of GFP molecules bound to single MBS-tagged mRNA is ~30 (*9, 28*). These results indicate that β-actin mRNA molecules do not multimerize in MEFs.

In neurons, several studies have suggested that large mRNP complexes contain many mRNAs based on their large size (*11, 13*) and the colocalization of different mRNA species (*29, 30*). However, recent reports challenged this view by suggesting neuronal mRNPs contain very few mRNA molecules (*31*) or have only a single mRNA (*32*). In order to investigate the stoichiometry of β-actin mRNA in neuronal mRNPs, we cultured hippocampal neurons from MCP×MBS mice and performed single molecule FISH (fig. S7) and live-cell imaging (Fig. 1C and E and fig. S9B). Both methods revealed that 3) the copy number of β-actin mRNAs in neuronal mRNPs are heterogeneous. The peak with the lowest fluorescent intensity (Fig. 1E) had a similar value as the single peak in MEFs (Fig. 1D) under the same imaging condition. The majority of neuronal mRNPs contained a single or low copy number of β-actin mRNA. However, it is possible that these particles contain many copies of different mRNA species that are not labeled.

Serum-induced localization of β-actin mRNA in primary fibroblasts

It was previously shown that addition of serum to starved chicken embryonic fibroblasts (CEFs) induced localization of β-actin mRNA into the leading lamellae within 2-5 min (*33*). In order to investigate the transport mechanism for RNA localization, we performed single particle tracking in primary MEFs before and after serum induction (fig. S6, Movie S2-5). Within a minute after serum addition, β-actin mRNA was localized in small patches (fig. S6B) and continuously redistributed along the leading edge (fig. S6, C and D). In the localized area, mRNA molecules showed mostly diffusive (blue tracks) or corralled motion (green tracks) with higher diffusion coefficients than in other regions. During the first 2 min of serum induction, the fraction of stationary mRNA (red tracks) decreased (fig. S6E), and the ensemble diffusion coefficient increased by ~25% (fig. S6, H and I). However, directed motion of mRNA was rarely observed throughout the localization process. These results suggest that serum-induced β-actin mRNA

localization in primary fibroblasts is mediated mainly by rapid release of stationary mRNA and redistribution in discrete cytoplasmic compartments by diffusion and entrapment.

Localization of β-actin mRNA in fibroblast requires intact actin filaments but not microtubules or intermediate filaments (*34*). In order to study the effect of the actin cytoskeleton on the movement of mRNA, we performed single particle tracking before and after the treatment with 10 μM Latrunculin A. The diffusion coefficient of mRNA increased upon disruption of microfilaments by Latrunculin A within 4 min (fig. S6J). Fusco *et al.* and Yamagishi *et al.* also reported that diffusion coefficients of mRNA increased after treating cells with swinholide and cytochalasin D, respectively (*9*, *35*). These data suggest that actin cytoskeleton serves a role in mRNA localization in fibroblast by restricting diffusion of mRNA to confined regions.

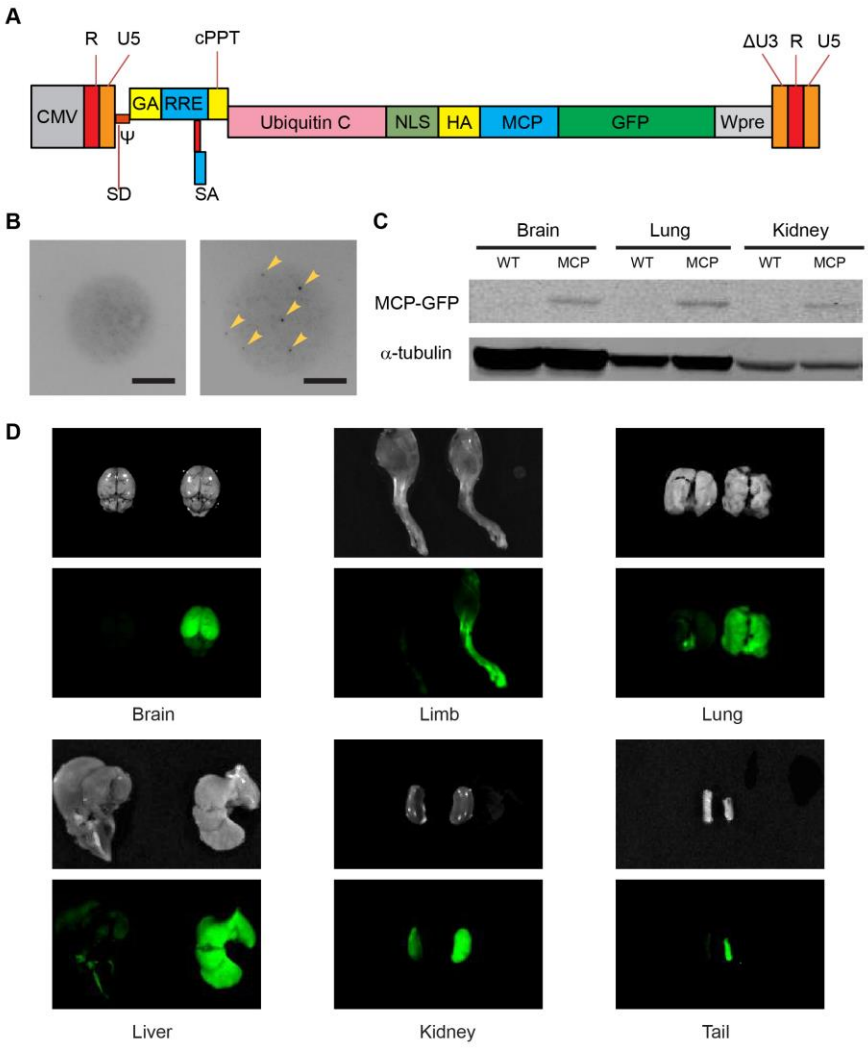

Fig. S1. Generation of the MCP mouse. (**A**) Schematic of the transfer construct used to prepare VSV-pseudotyped third generation HIV-l-derived lentiviral vectors. The self-inactivating (SIN) transfer construct expresses the genomic RNA from the cytomegalovirus (CMV) promoter and contains HIV-1 cis-acting sequences and an expression cassette for the transgene (NLS: nuclear localization signal, HA: hemagglutinin, MCP: MS2 capsid protein, GFP: green fluorescent protein) driven by the internal promoter Ubiquitin C. Abbreviations: Long terminal repeats (LTRs: U3-R-U5); the 5´ LTR of transfer construct is chimeric, with the enhancer-promoter of the CMV replacing the U3 region and the 3´ LTR has an almost complete deletion of the U3 region (delta U3). Splice donor and acceptor sites (SD and SA), the packaging sequence (psi), 5´ portion of *gag* gene with truncated reading frame including extended packaging signal (GA), Rev Response Element (RRE), central polypurine tract (cPPT), posttranscriptional regulatory element from the genome of the woodchuck hepatitis virus (Wpre). (**B**) DNA fluorescence in situ hybridization (FISH) on interphase spreads of C57BL/6J wild-type (WT) (left) and MCP founder number 4 (right) mouse macrophages using the MCP-GFP probe. The transgene integration loci appear as six bright fluorescent spots (arrowheads) in the image on the right side. Scale bars, 5 μm. (**C**) Western blot of tissue lysates from WT and MCP mice. (**D**) Whole organ images of WT (left) and MCP (right) mice. GFP fluorescence is observed in MCP mouse tissues.

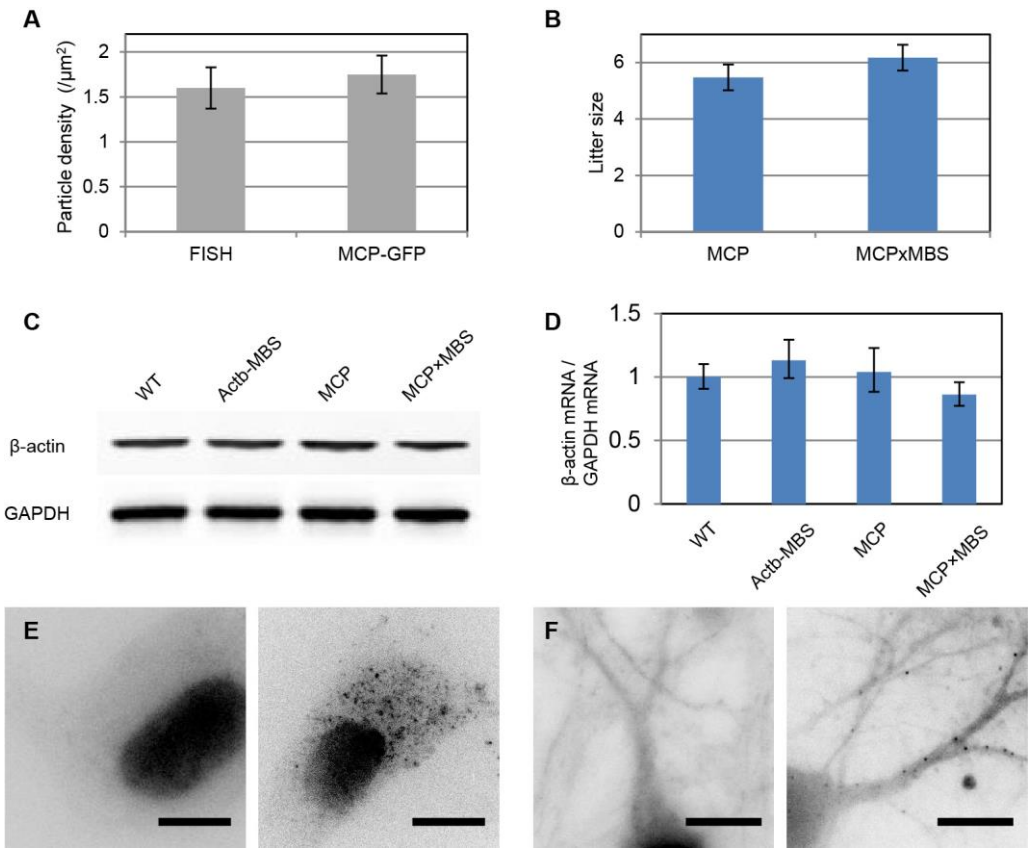

Fig. S2. Characterization of MCP×MBS mouse. (**A**) The density of β-actin mRNP particles detected by single molecule FISH (using MS2_LK51 probes) and MCP-GFP in fixed primary fibroblasts (n = 3 cells). There was no significant difference between the particle densities using the two methods (P > 0.1 by t test), suggesting that all MBS tagged β-actin mRNA molecules are labeled by MCP-GFP. (**B**) The litter sizes of MCP and MCP×MBS mice were similar to the mean litter size of C57BL mice (*36*). There was no significant difference in the litter size of MCP (n = 19) and MCP×MBS mice (n = 23; P > 0.1 by t test). Error bars represent standard errors of the mean (SEM). (**C**) Western blot of brain tissue lysates from WT, Actb-MBS, MCP, and MCP×MBS mice. The expression level of β-actin protein was similar in all four mouse strains. (**D**) qRT-PCR analysis of β-actin mRNA expression level relative to GAPDH mRNA. There was no statistically significant difference between the four mouse strains (n = 6 measurements of the samples pooled from three mice for each strain; P > 0.1 by ANOVA). Error bars represent standard deviation (SD). (**E** and **F**) Intensity inverted GFP fluorescence images of MEFs (E) and hippocampal neurons (F) from MCP (left) and MCP×MBS (right) mice. In MCP cells, MCP-GFP fusion protein is confined in the nucleus because of the nuclear localization sequence (NLS). In MCP×MBS cells, bright particles are visible in the cytoplasm. Scale bars, 10 μm.

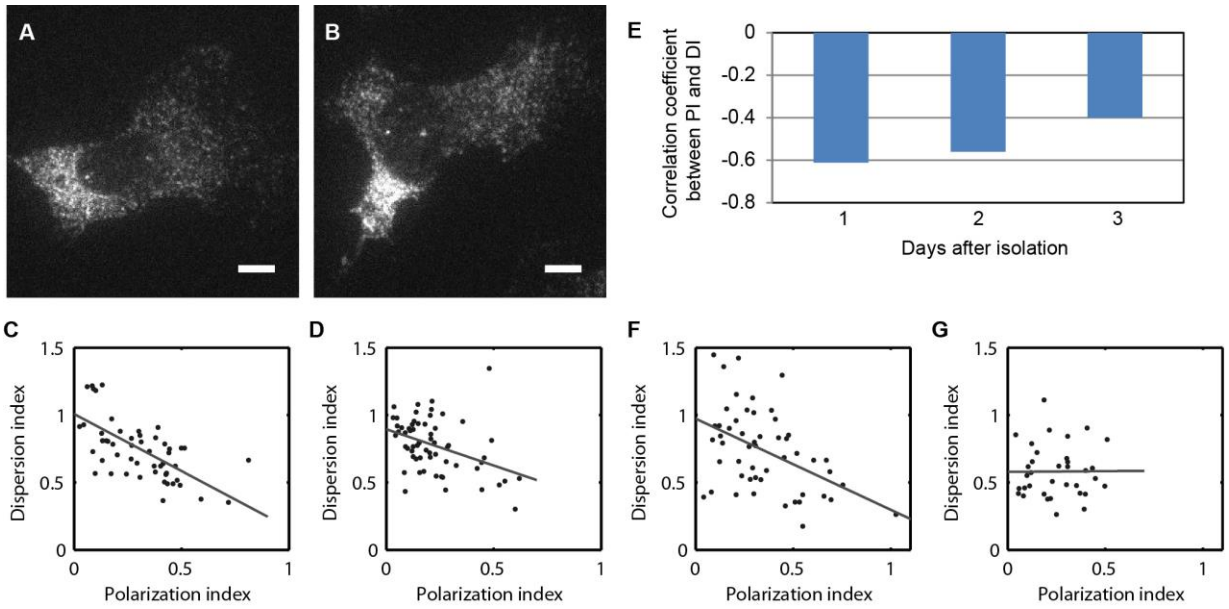

Fig. S3. Quantification of β-actin mRNA localization in primary fibroblasts. (**A** and **B**) Single molecule FISH images of WT (A) and MCP×MBS (B) fibroblasts hybridized with MBA UTR-1-5 probes. (**C** and **D**) Scatter plot of the polarization index (PI) and dispersion index (DI) of β-actin mRNAs in WT (C; n = 55 cells) and MCP×MBS (D; n = 62 cells) fibroblasts. The correlation coefficients between PI and the DI are -0.61 (C) and -0.40 (D), respectively. The negative correlation coefficients between PI and DI indicate the polarized localization of β-actin mRNA in both WT and MCP×MBS fibroblasts. Although the correlation coefficient was lower in MCP×MBS cells than in WT cells, this difference is within the variability of primary culture preparations. **(E)** The correlation coefficient between PI and DI decreased over time in the same preparation of WT primary fibroblasts, indicating gradual loss of β-actin mRNA localization in culture. (**F** and **G**) Scatter plot of the polarization index (PI) and dispersion index (DI) of β-actin mRNA in primary MEFs (F; n = 52 cells) and immortalized MEFs (G; n = 35 cells) from the Actb-MBS mice. The correlation coefficients between the PI and the DI are -0.46 (F) and 0.01 (G), respectively. No correlation between PI and DI indicates loss of β-actin mRNA localization in the immortalized MEF cell line.

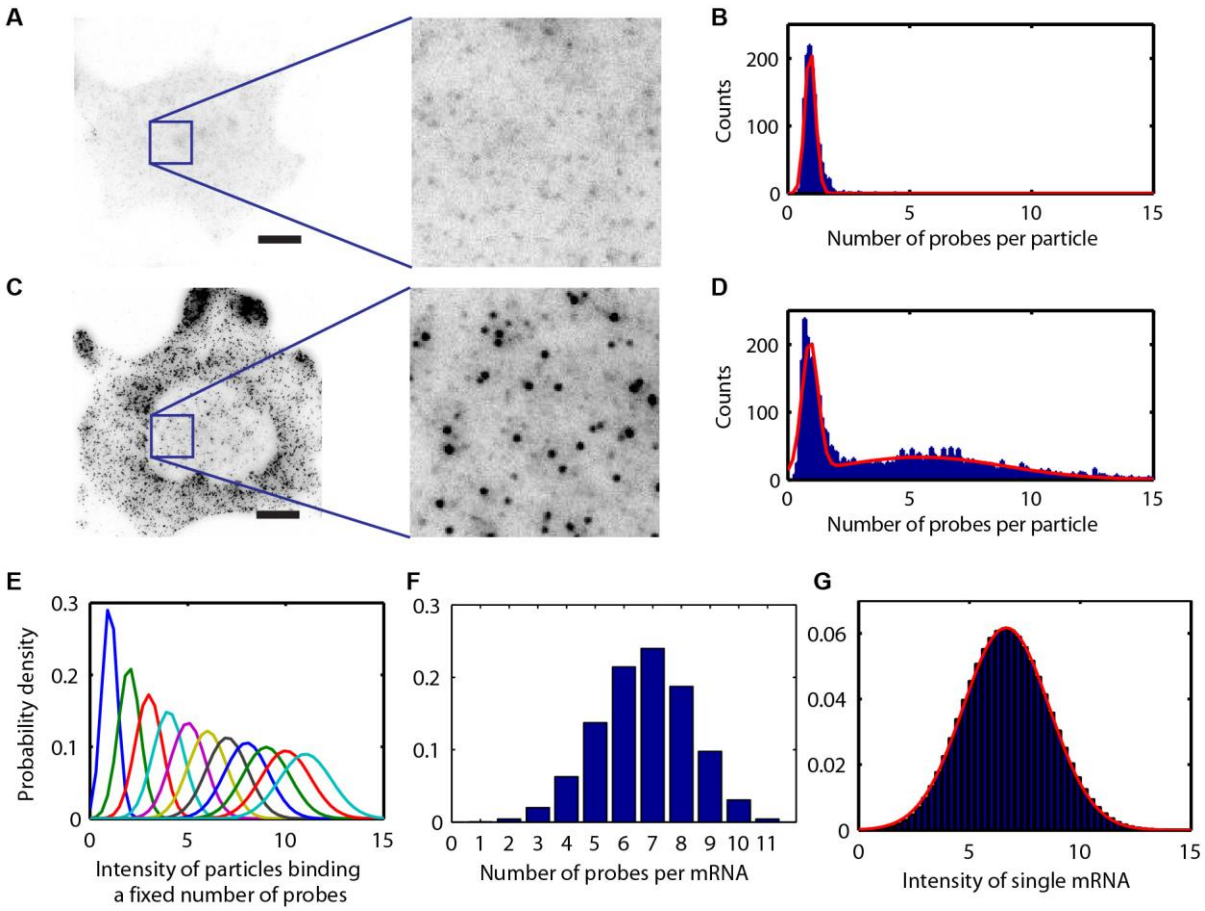

Fig. S4. Quantification of β-actin mRNA copy number per mRNP in fibroblasts. (**A**) Single molecule FISH image of an immortalized MEF from WT mouse showing non-specific binding of MS2_LK51 probes. Scale bar, 10 μm. (**B**) Intensity histogram of fluorescent spots detected in the WT MEF shown in (A). The red line represents a Gaussian fit. (**C**) Single molecule FISH image of an immortalized MEF from homozygous Actb-MBS mouse hybridized with MS2_LK51 probes. Scale bar, 10 μm. (**D**) Intensity histogram of fluorescent spots detected in the Actb-MBS MEF shown in (C). The spot intensities were normalized by the mean intensity of single probes. The red line represents a two-component Gaussian fit. (**E**) Theoretical distributions of particle intensities binding a fixed number of probes from 1 to 11. (**F**) The binomial distribution of probe numbers per mRNA with $N = 11$ and $p = 0.61$. (**G**) The intensity distribution of single mRNA calculated from the distributions shown in (E) and (F). The red line represents a Gaussian fit.

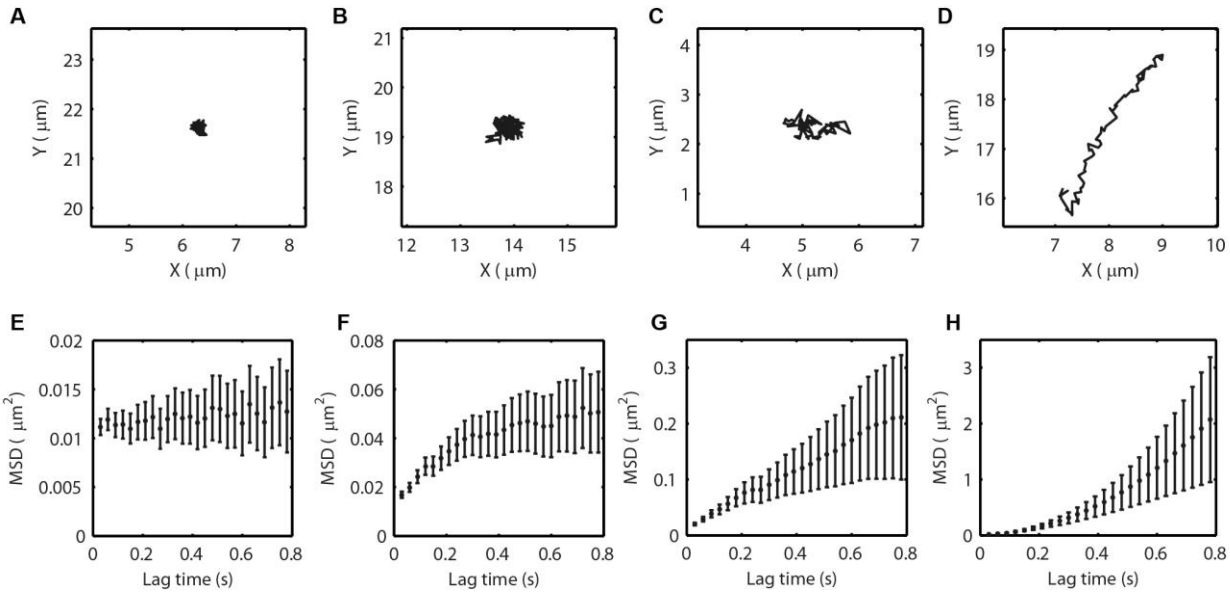

Fig. S5. Classification of motion types of β-actin mRNA. (**A**-**D**) Representative trajectories of mRNA showing stationary (A), corralled (B), diffusive (C), and directed (D) motions. (**E-H**) The mean squared displacement (MSD) versus lag time plots of the mRNA shown in (A), (B), (C), and (D), respectively.

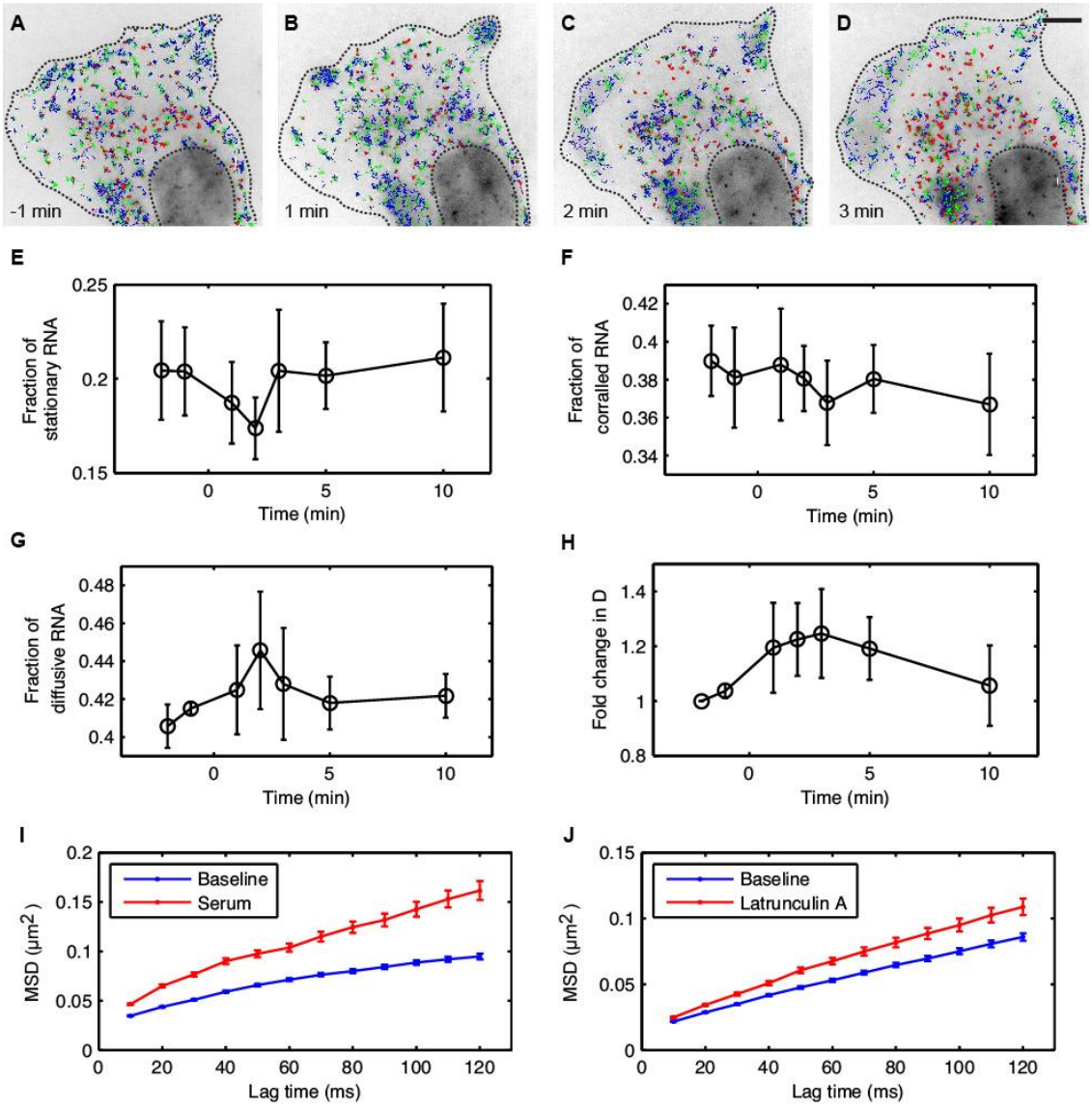

Fig. S6. Trafficking of β-actin mRNA during localization in primary MEFs. (**A**-**D**) Single particle tracking of β-actin mRNA in a primary MEF during localization upon serum induction. Trajectories of stationary (red), corralled (green), and diffusive (blue) mRNA during 6 s periods are overlaid on the time-averaged images at 1 min before (A), and 1 min (B), 2 min (C), and 3 min (D) after serum induction. Scale bar, 5 μm. (**E**-**G**) Changes in the fraction of stationary (E), corralled (F), and diffusive (G) motion during β-actin mRNA localization in primary MEFs. Transient release of stationary mRNA was observed during 2 min of serum induction. Error bars are SEM (n = 5 cells). (**H**) Fold changes in the ensemble diffusion coefficient of β-actin mRNA during serum-induced mRNA localization. The diffusion coefficient increased rapidly within 3 min after serum addition and decreased back to the baseline at a slower rate. Error bars represent SEM (n = 5 cells). (**I** and **J**) Mean squared displacement (MSD) of β-actin mRNA in the baseline and at 4 min after adding serum (I) or Latrunculin A (J).

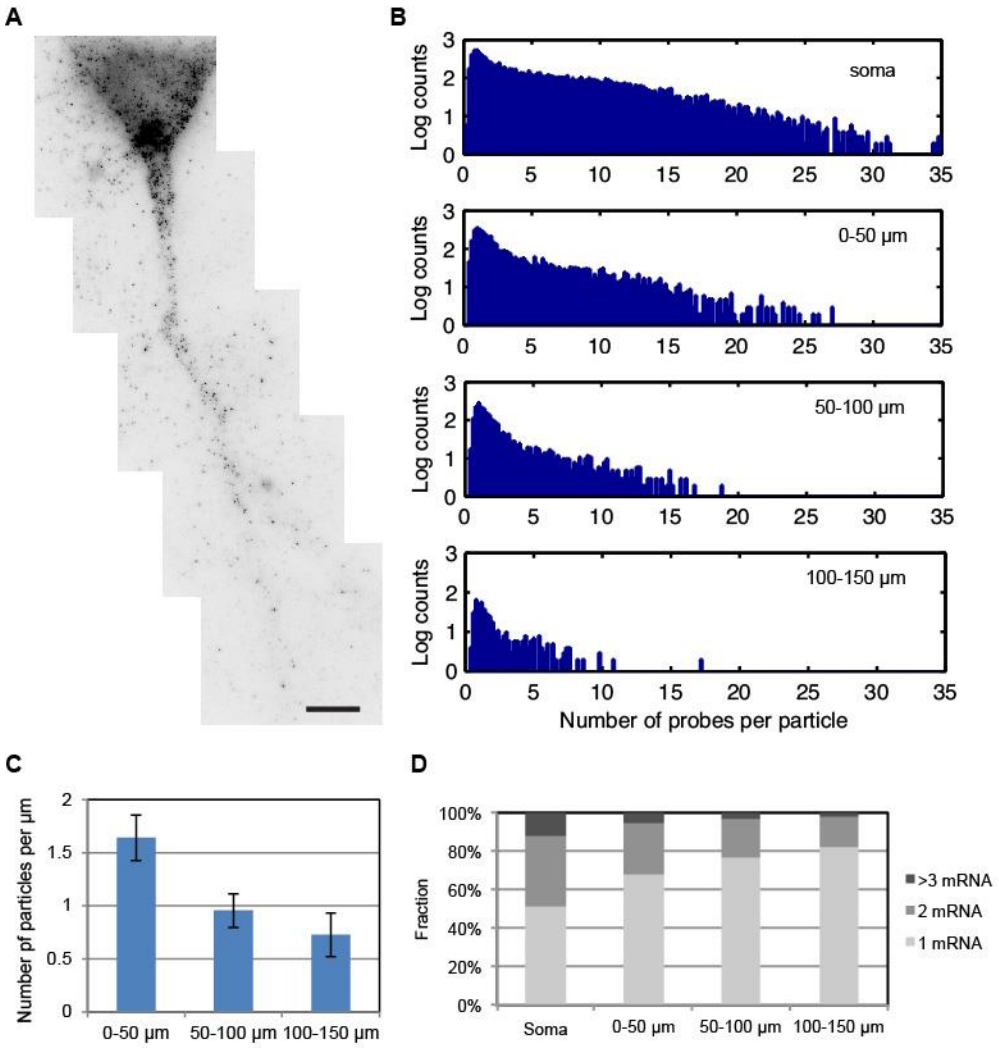

Fig. S7. Distribution of β-actin mRNA in hippocampal neurons cultured from MCP×MBS mice. (**A**) Single molecule FISH image of a 14 DIV hippocampal neuron hybridized with MS2_LK51 probe. Scale bar, 10 µm. (**B**) Histograms of probe number per fluorescent spot detected in the soma and dendritic segments at 0-50 µm, 50-100 µm, and 100-150 µm from the soma (data pooled from n = 24 neurons at DIV 14-21). The particle counts are shown in a logarithmic scale to make the population of mRNA particles more visible albeit the dominating number of nonspecifically bound single probes. (**C**) Linear density of β-actin mRNA particles detected in dendritic segments at 0-50 µm (n = 26), 50-100 µm (n = 18), and 100-150 µm (n = 8) from the soma. Error bars represent SEM. (**D**) Fraction of particles that contain 1 copy of β-actin mRNA (7 ± 3 probes), 2 copies of β-actin mRNA (14 ± 4 probes), and more than 3 copies of β-actin mRNA (> 18 probes) in the soma and dendritic segments at 0-50 µm, 50-100 µm, and 100-150 µm from the soma.

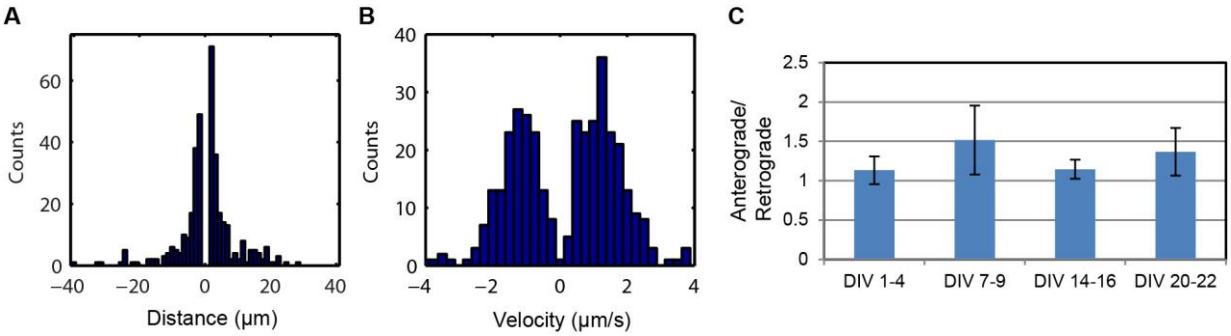

Fig. S8. Directed transport of β-actin mRNA in hippocampal neurons. (**A**) Histogram of travel distance by directed particles (data pooled from *n* = 14 neurons at DIV 14-16). Movements with travel distance less than 1.5 μm were excluded from the analysis. Positive distance corresponds to anterograde movement and negative distance corresponds to retrograde movement. (**B**) Velocity histogram of directed particles (data pooled from *n* = 14 neurons at DIV 14-16). Positive and negative velocity correspond to anterograde and retrograde movement, respectively. (**C**) Ratio of anterograde to retrograde movement of directed particles during development in culture. Error bars are SEM (*n* = 3-4 cultures).

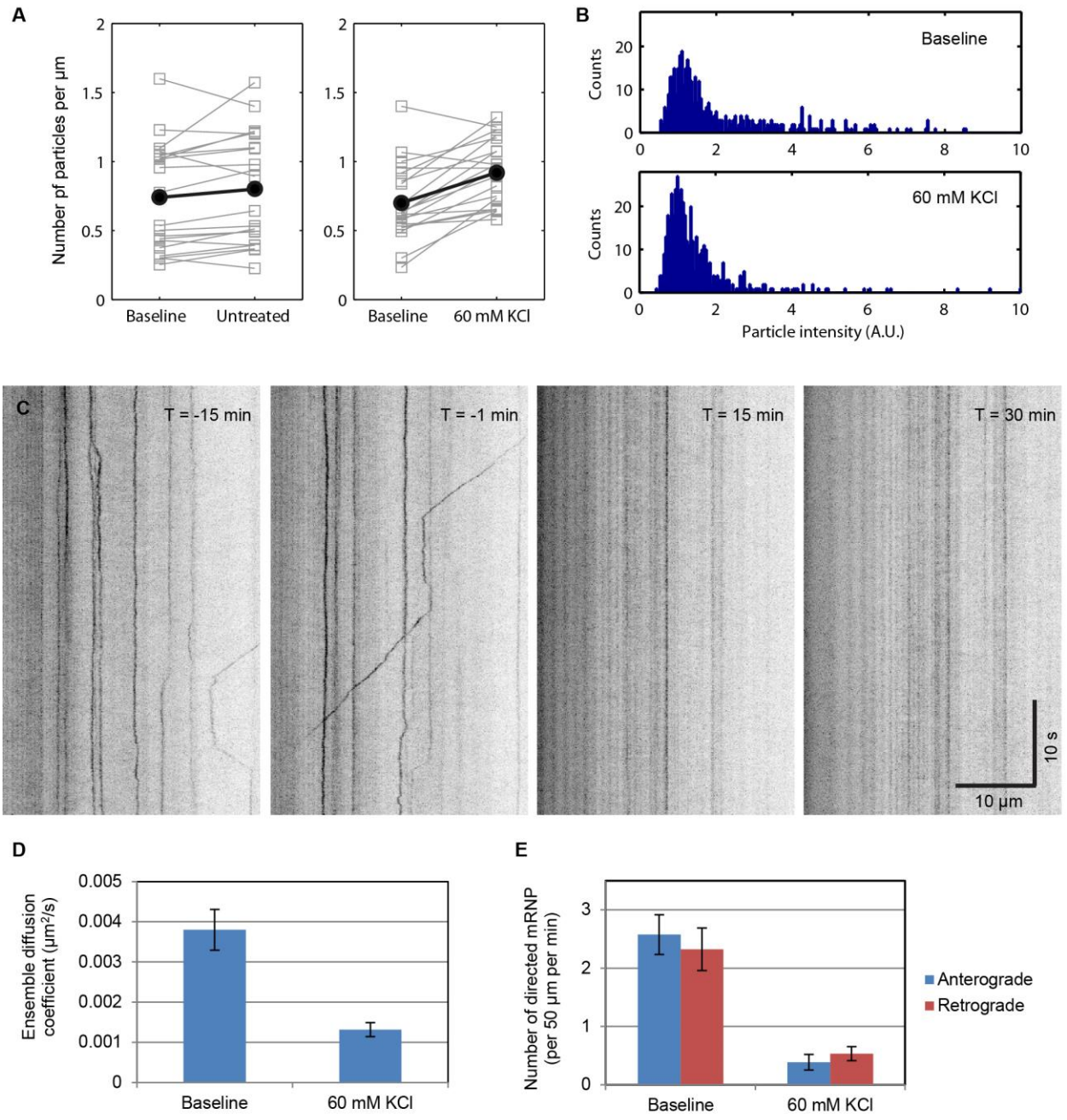

Fig. S9. Effect of KCl depolarization on β-actin mRNP movements in cultured neurons. (**A**) Effect of KCl depolarization on β-actin mRNA particle density in the dendrites (> 20 µm from the soma). Each line connects the particle density of the same dendrite before and at 20 min after treatment. Filled circles represent mean, open squares represent individual dendrites. The particle density significantly increased after KCl depolarization ($P < 0.01$; pairwise t test) but not in the untreated control (n = 20 dendritic segments from 9 neurons at DIV 15-19). (**B**) Intensity histograms of β-actin mRNP particles before (upper panel) and after depolarization (lower panel). After KCl depolarization, the amount of particles containing single β-actin mRNA increased while the number of particles with multiple copies of β-actin mRNA decreased (data pooled from 9 dendritic segments), suggesting that single β-actin mRNA molecules were

released from the common mRNP complexes upon stimulation. (**C**) Representative kymographs of particle movement in the baseline (T = -15 min and -1 min) and after KCl depolarization (T= 15 min and 30 min). The x-axis of the images represents the distance along the dendrite, and the y-axis represents the imaging time. (**D**) Ensemble diffusion coefficients of β-actin mRNPs before and at 10-15 min after depolarization (n = 6 neurons from 3 cultures). Diffusion of mRNPs slowed down significantly after depolarization ($P < 0.001$; pairwise t-test). Error bars represent SEM. (**E**) Effect of depolarization on directed motion of β-actin mRNP (n = 13 neurons from 3 cultures). The number of directed mRNPs decreased during 5-30 min after KCl depolarization in both anterograde and retrograde directions ($P < 0.001$; pairwise t test). Error bars represent SEM.

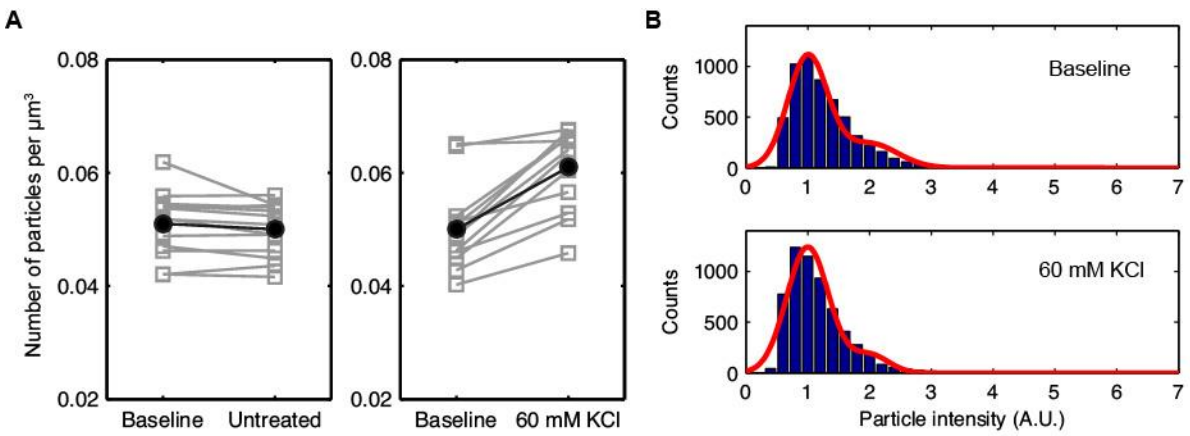

Fig. S10. Effect of KCl depolarization on β-actin mRNP in acute brain slices. (**A**) The density of β-actin mRNA particles in the CA1 apical dendritic regions increased significantly at 15-20 min after depolarization ($P < 0.001$; pairwise *t* test) but not in the untreated control (n = 12-13 regions from brain slices from 3 mice). Each line connects the particle density of the same region before and after treatment. Filled circles represent mean, open squares represent individual regions of interest. (**B**) Intensity histograms of β-actin mRNA particles in an acute brain slice before (upper panel) and after KCl depolarization (lower panel). Red lines show three-component Gaussian fit with fixed values for one and two mRNA intensities. After depolarization, the number of single mRNA increased from 81.8% (baseline) to 87.3% (after KCl depolarization), while the number of mRNPs containing multiple copies of β-actin mRNA decreased from 18.2% (baseline) to 12.7% (after KCl depolarization).

Supplementary Movie Captions:

Movie S1.

Movement of β-actin mRNA in a primary MEF cultured from MCP×MBS mouse shown in Fig. 1B. Time-lapse images were acquired at 33 fps for 6 s. Three frames were averaged for each image to reduce the noise in the movie. The movie is played at 3 times real speed.

Movie S2.

Movement of β-actin mRNA in a starved MEF shown in fig. S6A. Time-lapse images were acquired at 33 fps for 6 s. Three frames were averaged for each image to reduce the noise. The movie is played at 3 times real speed.

Movie S3.

Movement of β-actin mRNA in the MEF shown in fig. S6B at 1 min after adding 15% FBS following overnight starvation. Small patches of mRNA localization area appeared in the leading edge of the cell. β-actin mRNA molecules were diffusing much faster in the localization area than in other areas. Images were acquired at 33 fps for 6 s. Three frames were averaged for each image. The movie is played at 3 times real speed.

Movie S4.

Movement of β-actin mRNA in the MEF shown in fig. S6C at 2 min after adding 15% FBS. RNA molecules were diffusing rapidly in the localized area along the leading edge of the cell. Images were acquired at 33 fps for 6 s and three frames were averaged. The movie is played at 3 times real speed.

Movie S5.

Movement of β-actin mRNA in the MEF shown in fig. S6D at 3 min after adding 15% FBS. The mRNA localization area was expanded along the leading edge of the cell. While β-actin mRNA moved rapidly in the localized area, RNA molecules in the perinuclear region became slower or stationary. Images were acquired at 33 fps for 6 s and three frames were averaged. The movie is played at 3 times real speed.

Movie S6.

Movement of β-actin mRNA in a hippocampal neuron at DIV 15 shown in Fig. 1C. Most of β-actin mRNA were stationary or corralled. A few mRNA molecules showed directed transport in both anterograde and retrograde directions. Time-lapse images were acquired at 10 fps for 20 s. Two frames were averaged for each image in order to reduce the noise in the movie. The movie is played at 6 times real speed.

Movie S7.

Example of β-actin mRNA merging shown in Fig. 2A (first panel). Time-lapse images were acquired at 10 fps for 12 s. The movie is played at 3 times real speed.

Movie S8.

Example of β-actin mRNA splitting shown in Fig. 2B (first panel). Time-lapse images were acquired at 10 fps for 12 s. The movie is played at 3 times real speed.

References

1. S. Tyagi, Imaging intracellular RNA distribution and dynamics in living cells. *Nat. Methods* **6**, 331–338 (2009). doi:10.1038/nmeth.1321

2. E. Bertrand, P. Chartrand, M. Schaefer, S. M. Shenoy, R. H. Singer, R. M. Long, Localization of ASH1 mRNA particles in living yeast. *Mol. Cell* **2**, 437–445 (1998). doi:10.1016/S1097-2765(00)80143-4 Medline

3. C. Lois, E. J. Hong, S. Pease, E. J. Brown, D. Baltimore, Germline transmission and tissue-specific expression of transgenes delivered by lentiviral vectors. *Science* **295**, 868–872 (2002). doi:10.1126/science.1067081 Medline

4. T. Lionnet, K. Czaplinski, X. Darzacq, Y. Shav-Tal, A. L. Wells, J. A. Chao, H. Y. Park, V. de Turris, M. Lopez-Jones, R. H. Singer, A transgenic mouse for in vivo detection of endogenous labeled mRNA. *Nat. Methods* **8**, 165–170 (2011). doi:10.1038/nmeth.1551 Medline

5. T. M. Bunnell, B. J. Burbach, Y. Shimizu, J. M. Ervasti, β-Actin specifically controls cell growth, migration, and the G-actin pool. *Mol. Biol. Cell* **22**, 4047–4058 (2011). doi:10.1091/mbc.E11-06-0582 Medline

6. J. B. Lawrence, R. H. Singer, Intracellular localization of messenger RNAs for cytoskeletal proteins. *Cell* **45**, 407–415 (1986). doi:10.1016/0092-8674(86)90326-0 Medline

7. G. J. Bassell, H. Zhang, A. L. Byrd, A. M. Femino, R. H. Singer, K. L. Taneja, L. M. Lifshitz, I. M. Herman, K. S. Kosik, Sorting of β-actin mRNA and protein to neurites and growth cones in culture. *J. Neurosci.* **18**, 251–265 (1998). Medline

8. D. M. Tiruchinapalli, Y. Oleynikov, S. Kelic, S. M. Shenoy, A. Hartley, P. K. Stanton, R. H. Singer, G. J. Bassell, Activity-dependent trafficking and dynamic localization of zipcode binding protein 1 and β-actin mRNA in dendrites and spines of hippocampal neurons. *J. Neurosci.* **23**, 3251–3261 (2003). Medline

9. D. Fusco, N. Accornero, B. Lavoie, S. M. Shenoy, J. M. Blanchard, R. H. Singer, E. Bertrand, Single mRNA molecules demonstrate probabilistic movement in living mammalian cells. *Curr. Biol.* **13**, 161–167 (2003). doi:10.1016/S0960-9822(02)01436-7 Medline

10. K. Ainger, D. Avossa, F. Morgan, S. J. Hill, C. Barry, E. Barbarese, J. H. Carson, Transport and localization of exogenous myelin basic protein mRNA microinjected into oligodendrocytes. *J. Cell Biol.* **123**, 431–441 (1993). doi:10.1083/jcb.123.2.431 Medline

11. R. B. Knowles, J. H. Sabry, M. E. Martone, T. J. Deerinck, M. H. Ellisman, G. J. Bassell, K. S. Kosik, Translocation of RNA granules in living neurons. *J. Neurosci.* **16**, 7812–7820 (1996). Medline

12. C. P. Brangwynne, C. R. Eckmann, D. S. Courson, A. Rybarska, C. Hoege, J. Gharakhani, F. Jülicher, A. A. Hyman, Germline P granules are liquid droplets that localize by controlled dissolution/condensation. *Science* **324**, 1729–1732 (2009). doi:10.1126/science.1172046 Medline

13. A. M. Krichevsky, K. S. Kosik, Neuronal RNA granules: A link between RNA localization and stimulation-dependent translation. *Neuron* **32**, 683–696 (2001). doi:10.1016/S0896-6273(01)00508-6 Medline

14. A. R. Buxbaum, R. H. Singer, *Neuroscience 2012 Abstracts*, Program No. 240.01 (2012).

15. D. R. Larson, D. Zenklusen, B. Wu, J. A. Chao, R. H. Singer, Real-time observation of transcription initiation and elongation on an endogenous yeast gene. *Science* **332**, 475–478 (2011). doi:10.1126/science.1202142 Medline

16. A. M. Femino, F. S. Fay, K. Fogarty, R. H. Singer, Visualization of single RNA transcripts in situ. *Science* **280**, 585–590 (1998). doi:10.1126/science.280.5363.585 Medline

17. M. E. Greenberg, E. B. Ziff, L. A. Greene, Stimulation of neuronal acetylcholine receptors induces rapid gene transcription. *Science* **234**, 80–83 (1986). doi:10.1126/science.3749894 Medline

18. A. Follenzi, L. Naldini, Generation of HIV-1 derived lentiviral vectors. *Methods Enzymol.* **346**, 454–465 (2002). doi:10.1016/S0076-6879(02)46071-5 Medline

19. J. Roohi, M. Cammer, C. Montagna, E. Hatchwell, An improved method for generating BAC DNA suitable for FISH. *Cytogenet. Genome Res.* **121**, 7–9 (2008). doi:10.1159/000124374 Medline

20. K. Jaqaman, D. Loerke, M. Mettlen, H. Kuwata, S. Grinstein, S. L. Schmid, G. Danuser, Robust single-particle tracking in live-cell time-lapse sequences. *Nat. Methods* **5**, 695–702 (2008). doi:10.1038/nmeth.1237

21. S. Kaech, G. Banker, Culturing hippocampal neurons. *Nat. Protoc.* **1**, 2406–2415 (2006). doi:10.1038/nprot.2006.356

22. T. A. Pologruto, B. L. Sabatini, K. Svoboda, ScanImage: Flexible software for operating laser scanning microscopes. *Biomed. Eng. Online* **2**, 13 (2003). doi:10.1186/1475-925X-2-13 Medline

23. Y. Shav-Tal, X. Darzacq, S. M. Shenoy, D. Fusco, S. M. Janicki, D. L. Spector, R. H. Singer, Dynamics of single mRNPs in nuclei of living cells. *Science* **304**, 1797–1800 (2004). doi:10.1126/science.1099754 Medline

24. A. Kusumi, Y. Sako, M. Yamamoto, Confined lateral diffusion of membrane receptors as studied by single particle tracking (nanovid microscopy). Effects of calcium-induced differentiation in cultured epithelial cells. *Biophys. J.* **65**, 2021–2040 (1993). doi:10.1016/S0006-3495(93)81253-0 Medline

25. M. J. Saxton, K. Jacobson, Single-particle tracking: Applications to membrane dynamics. *Annu. Rev. Biophys. Biomol. Struct.* **26**, 373–399 (1997). doi:10.1146/annurev.biophys.26.1.373 Medline

26. H. Y. Park, T. Trcek, A. L. Wells, J. A. Chao, R. H. Singer, An unbiased analysis method to quantify mRNA localization reveals its correlation with cell motility. *Cell Rep.* **1**, 179–184 (2012). doi:10.1016/j.celrep.2011.12.009 Medline

27. D. Zenklusen, D. R. Larson, R. H. Singer, Single-RNA counting reveals alternative modes of gene expression in yeast. *Nat. Struct. Mol. Biol.* **15**, 1263–1271 (2008). doi:10.1038/nsmb.1514

28. B. Wu, J. A. Chao, R. H. Singer, Fluorescence fluctuation spectroscopy enables quantitative imaging of single mRNAs in living cells. *Biophys. J.* **102**, 2936–2944 (2012). doi:10.1016/j.bpj.2012.05.017 Medline

29. Y. Gao, V. Tatavarty, G. Korza, M. K. Levin, J. H. Carson, Multiplexed dendritic targeting of α calcium calmodulin-dependent protein kinase II, neurogranin, and activity-regulated

cytoskeleton-associated protein RNAs by the A2 pathway. *Mol. Biol. Cell* **19**, 2311–2327 (2008). doi:10.1091/mbc.E07-09-0914 Medline

30. F. Tübing, G. Vendra, M. Mikl, P. Macchi, S. Thomas, M. A. Kiebler, Dendritically localized transcripts are sorted into distinct ribonucleoprotein particles that display fast directional motility along dendrites of hippocampal neurons. *J. Neurosci.* **30**, 4160–4170 (2010). doi:10.1523/JNEUROSCI.3537-09.2010 Medline

31. M. Mikl, G. Vendra, M. A. Kiebler, Independent localization of MAP2, CaMKIIα and β-actin RNAs in low copy numbers. *EMBO Rep.* **12**, 1077–1084 (2011). doi:10.1038/embor.2011.149 Medline

32. M. Batish, P. van den Bogaard, F. R. Kramer, S. Tyagi, Neuronal mRNAs travel singly into dendrites. *Proc. Natl. Acad. Sci. U.S.A.* **109**, 4645–4650 (2012). doi:10.1073/pnas.1111226109 Medline

33. V. M. Latham Jr., E. H. Kislauskis, R. H. Singer, A. F. Ross, β-actin mRNA localization is regulated by signal transduction mechanisms. *J. Cell Biol.* **126**, 1211–1219 (1994). doi:10.1083/jcb.126.5.1211 Medline

34. C. L. Sundell, R. H. Singer, Requirement of microfilaments in sorting of actin messenger RNA. *Science* **253**, 1275–1277 (1991). doi:10.1126/science.1891715 Medline

35. M. Yamagishi, Y. Ishihama, Y. Shirasaki, H. Kurama, T. Funatsu, Single-molecule imaging of β-actin mRNAs in the cytoplasm of a living cell. *Exp. Cell Res.* **315**, 1142–1147 (2009). doi:10.1016/j.yexcr.2009.02.009 Medline

36. M. Festing, Some aspects of reproductive performance in inbred mice. *Lab. Anim.* **2**, 89–100 (1968). doi:10.1258/002367768781035430